Research in Astronomy and Astrophysics, 22:075007 (11pp), 2022 July https://doi.org/10.1088/1674-4527/ac6fb8

On the Relation Between Coronal Green Line Brightness and Magnetic Fields Intensity

Xue-Fei Zhang[1,2], Yu Liu[1,2,3], Ming-Yu Zhao[1], Teng-Fei Song[1,2], Jing-Xing Wang[1], Xiao-Bo Li[1], and Zi-Han Li[1,3]
[1] Yunnan Observatories, Chinese Academy of Sciences, Kunming 650011, China; zhangxuefei@ynao.ac.cn
[2] University of Chinese Academy of Sciences, Beijing 100049, China; lyu@ynao.ac.cn
[3] Yunnan Normal University, School of Physics and Electronic Information, Kunming 650000, China
Received 2022 March 4; revised 2022 April 22; accepted 2022 May 3; published 2022 June 14

Abstract

Two-dimensional (2D) solar coronal magnetogram is difficult to be measured directly until now. From the previous knowledge, a general relation has been noticed that the brighter green-line brightness for corona, the higher coronal magnetic field intensity may correspond to. To try to further reveal the relationship between coronal green line brightness and magnetic field intensity, we use the 2D coronal images observed by Yunnan Observatories Green-line Imaging System (YOGIS) of the 10 cm Lijiang coronagraph and the coronal magnetic field maps calculated from the current-free extrapolations with the photospheric magnetograms taken by Helioseismic and Magnetic Imager (HMI) on board the Solar Dynamics Observatory (SDO) spacecraft. In our analysis, we identified the coronal loop structures and construct two-dimensional maps of the corresponding magnetic field intensity in the plane of the sky (POS) above the limb. We derive the correlation coefficients between the coronal brightness and the magnetic field intensity for different heights of coronal layers. We further use a linear combination of a Gaussian and a quadratic profile to fit the correlation coefficients distribution, finding a largest correlation coefficient of 0.82 near 1.1 $R_{\odot}$ (solar radii) where is almost the top of the closed loop system. For the small closed loop system identified, the correlation coefficient distributions crossing and covering the loop are calculated. We also investigate the correlation with extended heliocentric latitude zones and long period of one whole Carrington Rotation, finding again that the maximum correlation coefficient occurs at the same height. It is the first time for us to find that the correlation coefficients are high (all are larger than 0.8) at the loop-tops and showing poor correlation coefficients with some fluctuations near the feet of the coronal loops. Our findings indicate that, for the heating of the low-latitude closed loops, both DC (dissipation of currents) and AC (dissipation of Alfvén and magnetosonic waves) mechanisms should act simultaneously on the whole closed loop system while the DC mechanisms dominate in the loop-top regions. Therefore, in the distributions of the correlation coefficients with different heights of coronal layers, for both large- and small-scale latitude ranges, the coefficients can reach their maximum values at the same coronal height of 1.1 $R_{\odot}$, which may indicate the particular importance of the height of closed loops for studying the coupling of the local emission mechanism and the coronal magnetic fields, which maybe helpful for studying the origin of the low-speed solar wind.

Key words: Sun: magnetic fields – Sun: corona – Stars: coronae – Sun: activity – Sun: atmosphere – Sun: coronal mass ejections (CMEs) – Sun: fundamental parameters – Sun: heliosphere – Sun: UV radiation

1. Introduction

It is quite clear that the solar and stellar activities should be highly associated with their complicated magnetic field structures and evolutions (Sakurai 1981; Klimchuk 2002; Gregory et al. 2010, 2012). The coronal magnetic field gives information on the physical conditions of the sources, such as the sunspots, hot corona, solar eruptions and large-scale coronal loop structures (Brooks et al. 2021). Therefore, routine and accurate measurements of the coronal magnetic field are crucial for the identification of the causes of various violent eruptions, the explanation of coronal heating mechanism (Ji et al. 2012; Nived et al. 2022) and the acceleration mechanism of solar wind (Stakhiv et al. 2015, 2016), as well as the origin of the solar magnetic field (Lin & Forbes 2000; Shen et al. 2022).

The coronal optical radiation intensity is usually very weak and decreases sharply with height (e.g., Habbal et al. 2010; Liang et al. 2021; Liu et al. 2021). It is an extremely difficult task to measure the coronal magnetic field in the optical bands with high precision. Indirect methods for diagnosing coronal magnetic field have been developed such as extrapolation from the photospheric magnetograms (e.g., Wiegelmann & Sakurai 2021); NIR or UV coronal spectropolarimetric signatures measurements (e.g., Lin et al. 2000; Liu & Lin 2008; Lin 2009;

Liu 2009; Liu & Shen 2009; Qu et al. 2017; Chen et al. 2018; Zhao et al. 2019; Yang et al. 2020b; Chen et al. 2021a); combination of magnetohydrodynamic (MHD) and extreme ultraviolet (EUV) observations (e.g., Jiang et al. 2013; Shen et al. 2018; Zhu & Wiegelmann 2019; Chen et al. 2020; Zhao et al. 2021); estimation from wave properties and coronal oscillations (e.g., Sakurai et al. 2002; Tian et al. 2012; Shen et al. 2014; Nakariakov & Kolotkov 2020; Zhu et al. 2021; Ji et al. 2021); relying on the radio imaging (Tan et al. 2016; Yu et al. 2020). Recently, the measurement developed by using the magnetic-field-induced transition (MIT) technique seems potential and still under developing (Li et al. 2015, 2016; Chen et al. 2021b). Although these methods are now widely used for investigating coronal magnetism, it is imperative to conduct some easier ways to quickly estimate the coronal magnetic field from routine observations.

The coronal green line (530.3 nm) gives rise to the strongest forbidden line emission in the coronal spectrum. The first spectral results of the coronal green line was reported to be measured on nineteenth century during total solar eclipse expeditions (Wilson 1869). The large-scale coronal temperature and green-line intensity distribution appear to be closely associated with the underlying photospheric magnetic field structure and intensity (Guhathakurta et al. 1993; Wang et al. 1997), which indicates that the characteristics of the coronal green line and the coronal magnetic field should be relevant in some degree, but the point-to-point relation between them is rather unclear. It is found that the coronal green line brightness is particularly sharp around active regions, and reaches its maximum in the vicinity of the sunspot formation zone (Badalyan & Obridko 2006). Statistically, the coronal green line brightness varies with latitude and solar cycle phase, and the correlation coefficients for the coronal green line brightness and the magnetic field strengths on various scales show obvious cyclic character as a function of latitudes (Guhathakurta et al. 1992, 1993). The larger values of brightness at the poles appear during the maximum of the activity cycle, while at the equator during the cycle minimum (Badalyan & Obridko 2004). However, these statistical results do not show further observational results for the general relationship at different coronal heights.

In this work, we use the data taken from the 10 cm Lijiang coronagraph YOGIS system (or, NOGIS, defined by Ichimoto et al. 1999) to study in details the relationship of the local coronal green line intensity and the corresponding theoretical coronal magnetic field intensity. The analysis steps of this paper are as follows:

1. To construct a two-dimensional map of the magnetic field intensity in the POS, we use the potential-field source-surface (PFSS) extrapolation model;
2. To map the distribution of the coronal green line brightness at various radial direction, we use the two-dimensional images from YOGIS;
3. To extract and identify the coronal arched structures above the solar limb in the two-dimensional coronal green line images with a coronal loop identification approach;
4. To investigate the correlation between the coronal line brightness and magnetic field intensity near the identified coronal arched structure, we analysis the correlation coefficient distributions with respect to different coronal heights. We investigate the correlation between the coronal loop brightness and the magnetic field intensity and its distribution along the coronal loop. For comparison, we extend the calculations statistically for larger scale of latitude zones and for a larger timescale covering the entire Carrington Rotation (CR) 2143;
5. Finally, we fit the profile of the correlation coefficients distribution, in order to find some particular coronal heights where the coronal emission well consistent with the coronal magnetic fields.

In the following, we describe our observations in Section 2. An analysis and discussion of the correlation with the radial heights above the solar limb are presented in Section 3. Concluding remarks are given in Section 4.

2. Instrument and Data Analysis

During 2013, with the collaboration of NAOJ, the Norikura 10 cm coronagraph tube (Ichimoto et al. 1999) was renovated and successfully installed at the Lijiang Station of Yunnan Observatories (3200 m, E:100°01′4″, N:26°41′42″, IAU code: 044). The Lijiang Station is a low-latitude and high-altitude site with low-level sky scattered light and good atmospheric seeing condition (Zhao et al. 2014, 2018; Xin et al. 2020). Our statistical results of the sky background brightness measurement at the Lijiang Station show that the average sky brightness in optical bands is under 20 millionths per air mass when the sky is clear, suitable for a coronagraph to observe the structures and dynamics of the corona. It should be noted that this 10 cm coronagraph has kept the longest record of the coronal green-line observations in the world (Sakurai 2012).

The YOGIS system supplies coronal data with a typical field-of-view of $64' \times 64'$ (about 2.0 $R_\odot$ in x and y directions) and minimum height of 1.03 $R_\odot$ from the photosphere, which is suitable for observing the inner coronal configuration in time sequence. In 2013 the coronal images were recorded digitally by a CCD camera (1024×1024 pixel array) (Ichimoto et al. 1999). The raw data were preprocessed following the standard reduction procedure for calibration. Each frame has been corrected using the corresponding dark and flat fields, and the sky scattered light is subtracted from the continuum intensity. The data were taken during 2013 November when it was during

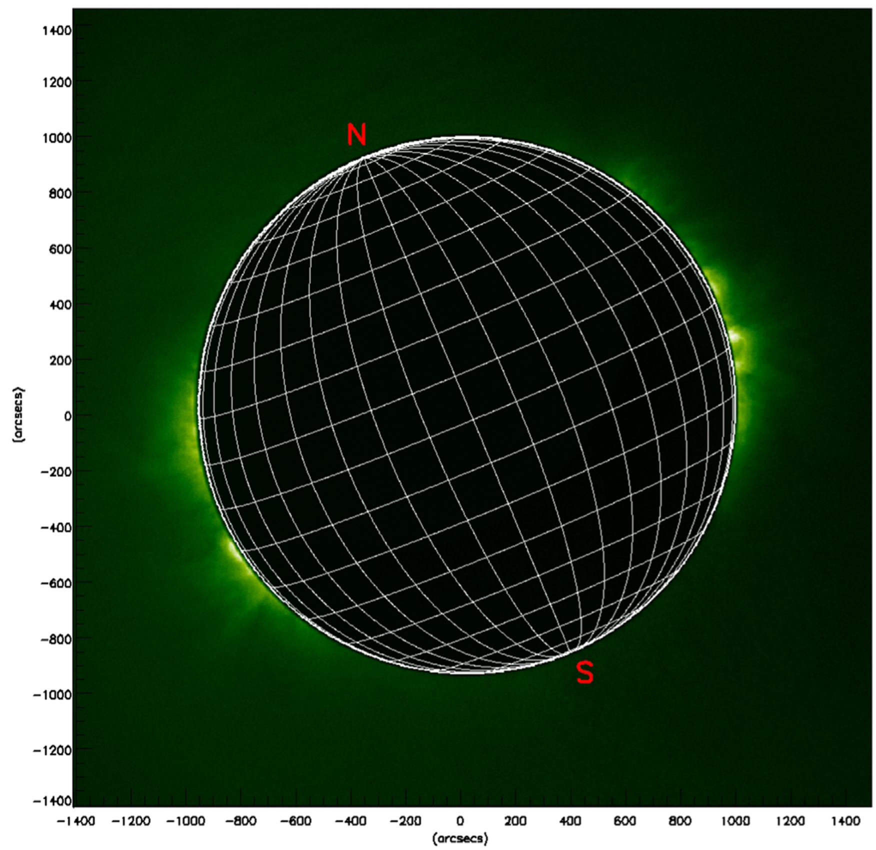

Figure 1. YOGIS observation from the Lijiang Station on 2013 November 15 (06:32 UT) in 5303 Å. The edge of the occulting disk is 1.03 $R_\odot$. As viewed from the Earth, solar east is to the left and west to the right, "N" and "S" represent the north and the south pole of the Sun, respectively.

dry season and some coronal features like low-lying closed and high open loops were obvious above solar limbs in λ 5303 Å.

Figure 1 shows the full FOV observation of YOGIS from the Lijiang Station on 2013 November 15. The clear coronal structure is distributed in low latitudes on the east and west sides of the Sun. The obvious arched structures near a low-latitude complex active region centered at latitude 10° in the south hemisphere above the west limb (as viewed from the Earth, the west is to the right). Several days ago, the active region was in a simple bipolar configuration from the observation of the Atmospheric Imaging Assembly (AIA; Lemen et al. 2012; Pesnell et al. 2012) and SDO/HMI (Xu et al. 2016).

The coronal magnetic fields are calculated from the PFSS model based on the synoptic magnetograms. The PFSS package can be available in the Solar SoftWare (SSW) (Schrijver & De Rosa 2003). We calculate the total magnetic field strengths B (the square root of the sum of the squared radial B_r and tangential B_t components; in G) in the plane of the sky, and compare them with the coronal intensity I in unit of the CCD digital readout. The data spatial resolutions of the magnetic field B and the coronal intensity I have been set the same. The coronal magnetic fields are derived in a spherical shell spanning radial distance up to 2.50 solar radii. We transfer and obtain the distribution of the total magnetic field intensity in polar coordinates. Next, the image data are interpolated according to the pixel resolution, in which the height is normalized by solar radii. Then, the image is transformed from polar coordinates to Cartesian coordinates. In this way, we construct a two-dimensional map of the magnetic field intensity in the POS with the same spatial resolutions as the coronal intensity observations of YOGIS from 1.03 to 1.3 $R_\odot$ in Figure 2.

In this work, all the calculations are made within a height range of 1.04−1.28 $R_\odot$. The heliocentric heights of them from below are 1.049, 1.067, 1.086, 1.103, 1.123, 1.143, 1.164, 1.186, 1.209, 1.232, 1.257, 1.282 $R_\odot$, respectively. The first region we will analyze is the active region with a clear corona structure on the western of the Sun. Figure 3 shows the layers of every radial coronal height in yellow. The edge of the dark occulting disk is at 1.03 $R_\odot$. There are 72 points evenly distributed in each yellow line. A coronal loop identification method based on the phase congruency theory (Li et al. 2017) is used to extract the particular arched loop

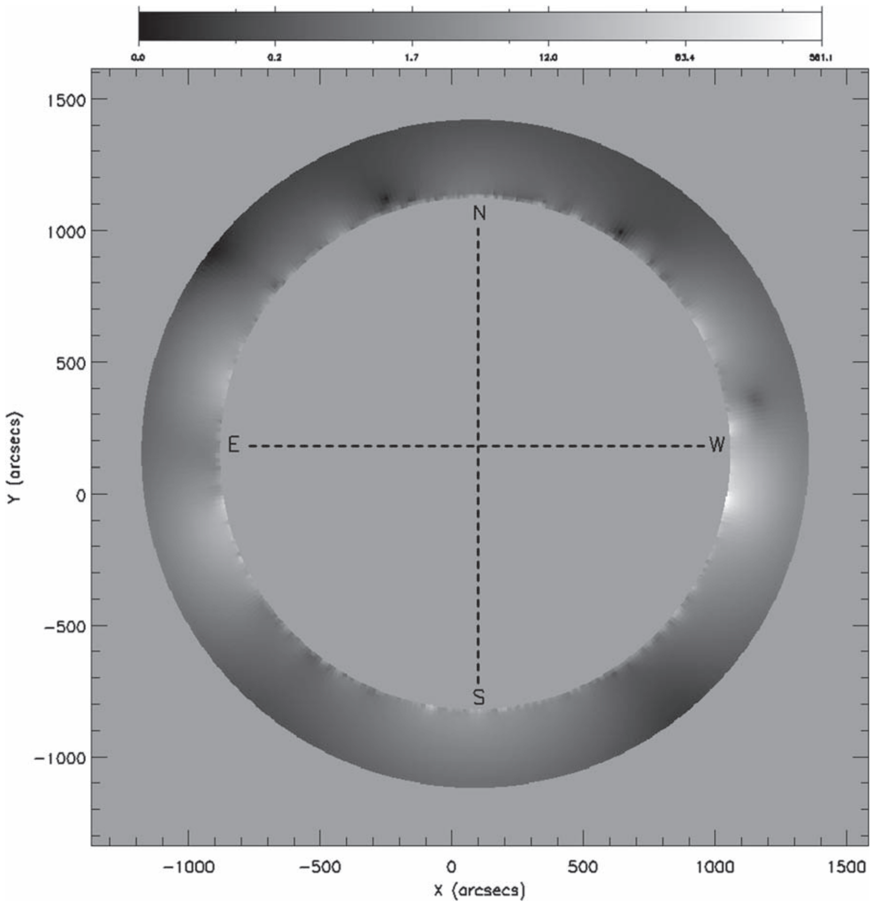

Figure 2. We construct a 2D image of the magnetic field intensity in the POS, the size of the spatial resolution is consistent with that of the YOGIS images.

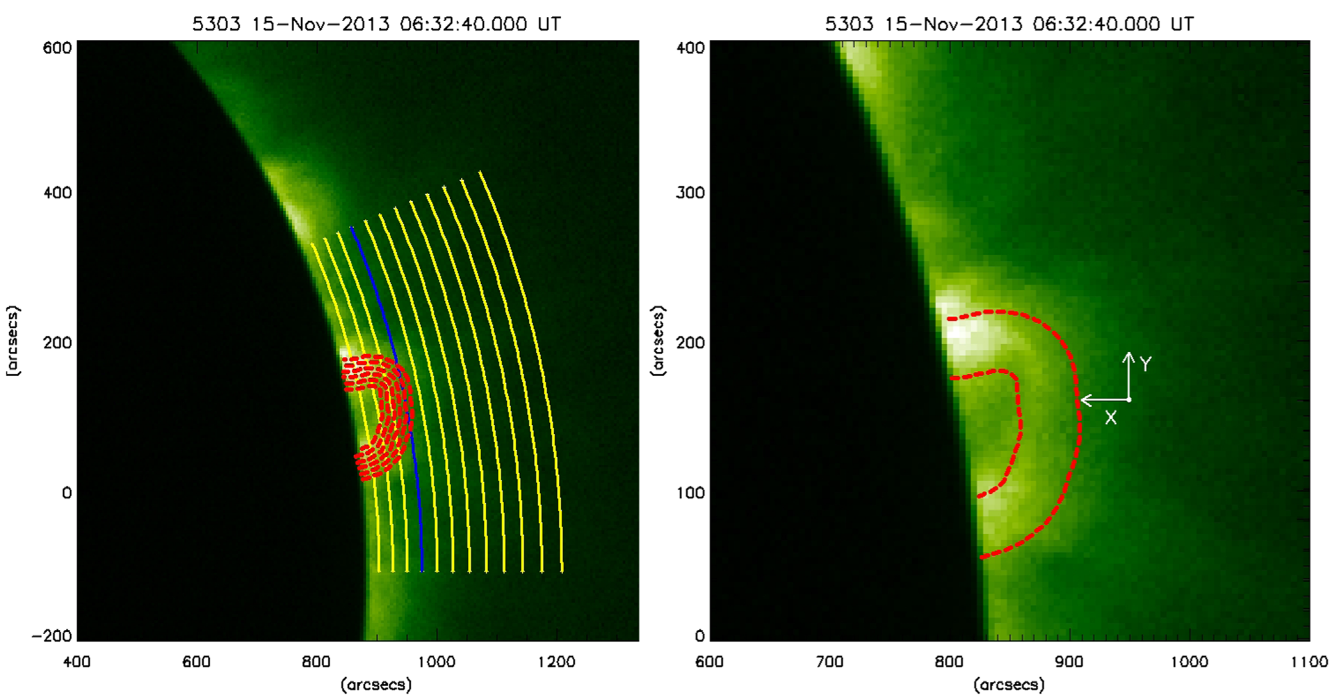

Figure 3. Left: layers to be calculated and compared, shown in yellow. The blue line shows the layer of 1.103 $R_{\odot}$ where is also the top of the particular closed loop (in red dotted line). Right: the identified coronal loops based on the YOGIS image, with Y and X for the direction along and perpendicular to the loop axis, respectively.

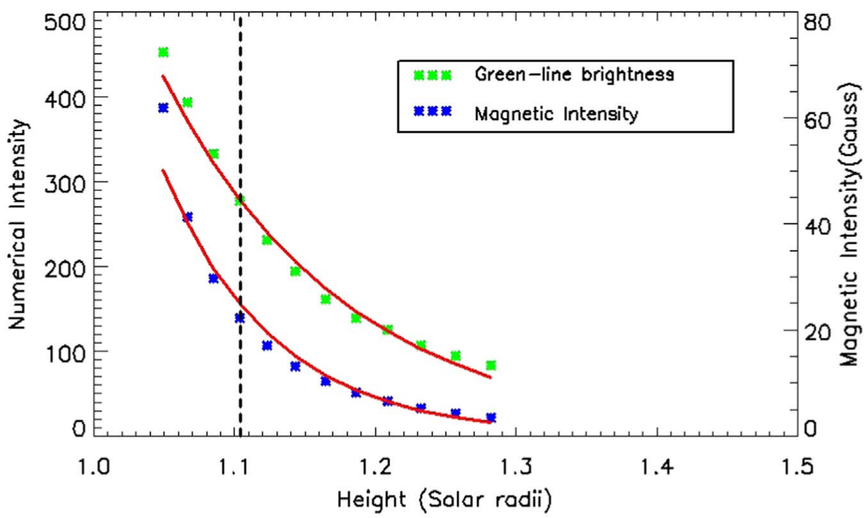

Figure 4. The distributions of the coronal green line brightness (green points) and the magnetic field intensity (blue points) with height. Each point represents the mean value of each yellow line in Figure 3 . The vertical dashed line shows the layer (at 1.103 $R_{\odot}$) near the loop top in Figure 3. The red lines are the fitted results.

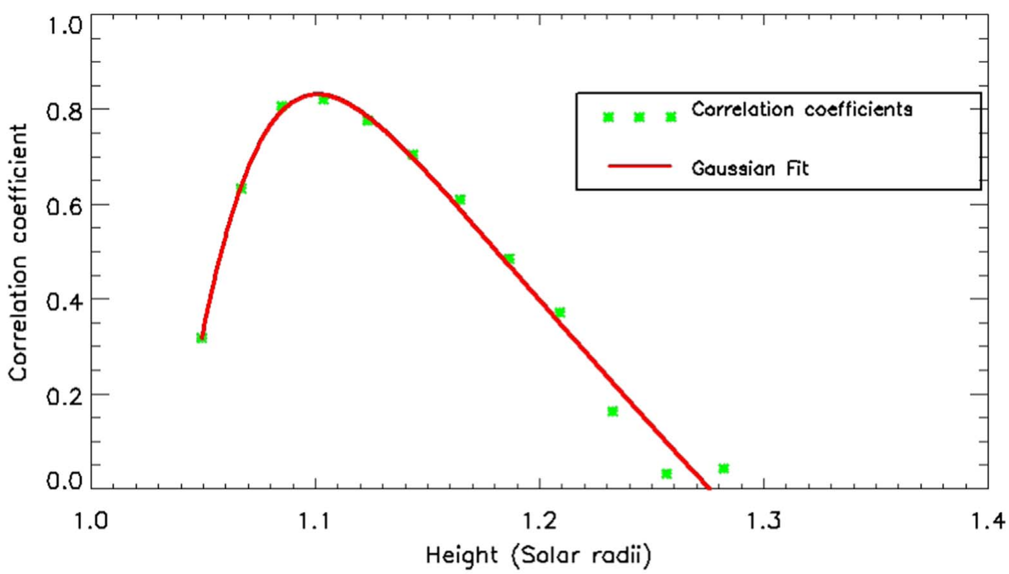

Figure 5. Correlation coefficients between the coronal green line brightness and the magnetic field intensity with height for the 12 yellow lines in Figure 3. The red line indicates the fitted profile by a linear combination of a Gaussian and a quadratic function.

system in Figure 1. The red dotted line represents the trajectory of the identified coronal loops. On the top of this red loop system a thick blue curve is plotted to represent the location of layer 1.103 $R_{\odot}$. The process of the coronal loop identification starts from one set of footpoints to the other one. The right panel in Figure 3 shows the identified results of the coronal loops based on YOGIS image in Figure 1. The *Y*-axis is along the direction of the loops (red dotted lines in Figure 3), and the coronal loop width between the two red dotted lines (*X*-axis direction) is 10 pixels in our calculation. It is demonstrated in red and its two footpoints cover nearly 10° in latitude at the limb.

In the following, we compare the magnetic field intensity derived from the PFSS model with the coronal brightness observed by YOGIS. Figure 4 shows the variations of the mean coronal brightness and the magnetic field intensity with height in Figure 3 each yellow line, the fitted curves are plotted as red lines. Each point represents an average value for each layer, which is the value of the coronal brightness and magnetic field intensity corresponding to each yellow line extracted from

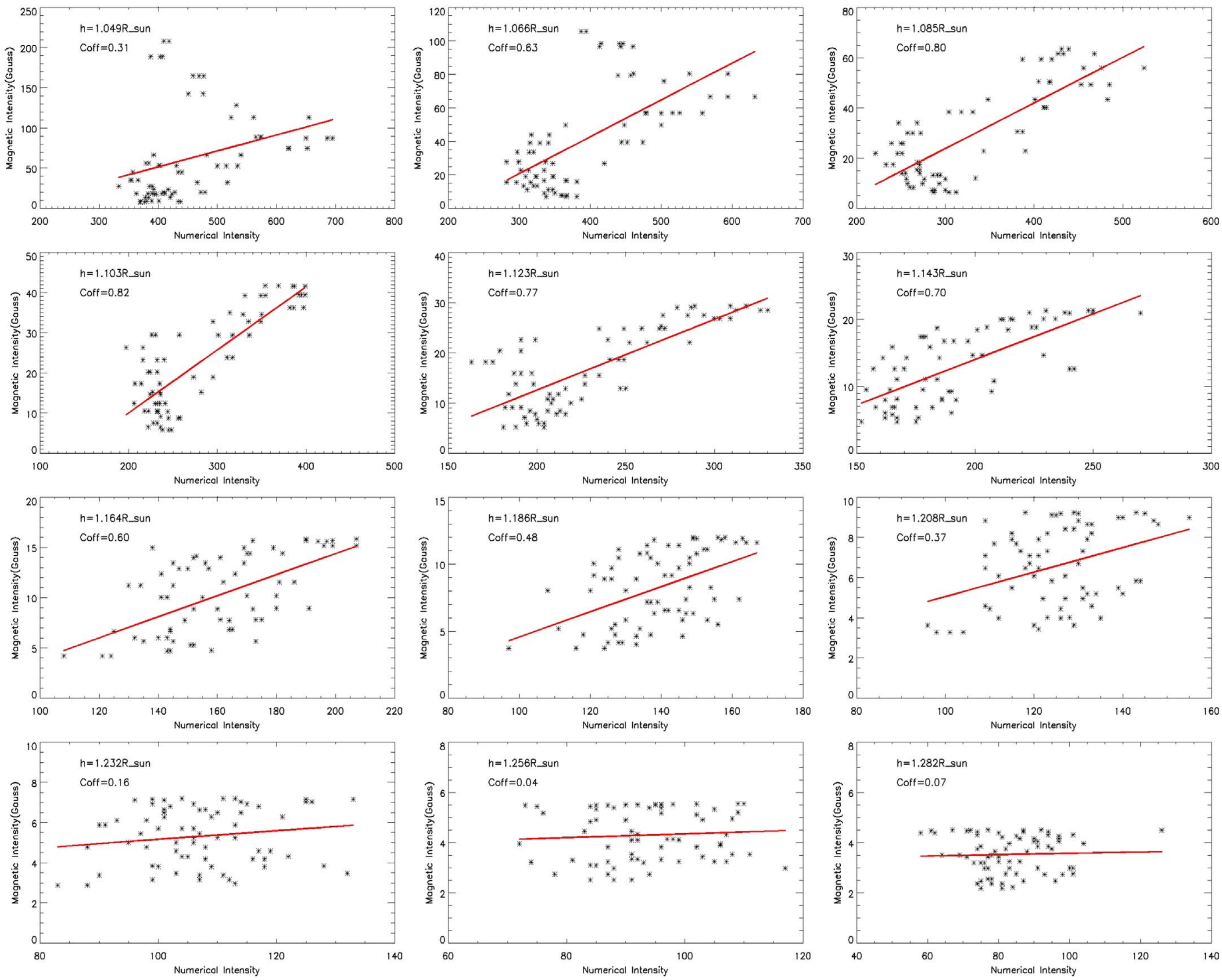

Figure 6. Plots of the coronal green line brightness against the coronal magnetic field intensity for the 12 layers in yellow in Figure 3. "Coff" is the Pearson Correlation Coefficient between the brightness and the magnetic field intensity. The red line in each frame indicates the fitted linear profile.

Figures 1 and 2, respectively. Similar trend can be noticed for the two parameters. Both the coronal brightness and the magnetic field intensity, from 1.049 $R_{\odot}$ to 1.28 $R_{\odot}$, show a quick decrease with the height increased. However, the decrease rate of the brightness seems slower than the magnetic field intensity. According to the fitting results, the coronal brightness is best fitted by the function: $y_1 = A_1 e^{-7.6x}$; while the coronal magnetic field intensity is best fitted by: $y_2 = A_2 e^{-12.6x}$, where A_1 and A_2 are constants. We note that the decreasing rate of the observed brightness at low heights are slower than but comparable to that of the extrapolated intensity, which agrees with the recent results of Landi et al. (2020) from Hinode/EUV Imaging Spectrometer (EIS) data diagnostic technique for corona above active regions.

3. Results

In Figure 5, we show the correlation coefficients variations with respect to heights in each yellow line. Here we fit the coefficients profile by computing a non-liner least-squares fit to a function $f(x)$ with six parameters. $f(x)$ is a linear combination of a Gaussian and a quadratic function: $f(x) = A_0 e^{\frac{-z^2}{2}} + A_3 + A_4 x + A_5 x^2$, where $z = \frac{x - A_1}{A_2}$. The six parameters represent the height ($A0$), the center position ($A1$), and the width ($A2$) of the Gaussian function, the constant term ($A3$), the linear term ($A4$), and the quadratic term ($A5$), respectively. The line profiles do not show explicit evidence of multi-components and the fits generally seem to be satisfactory.

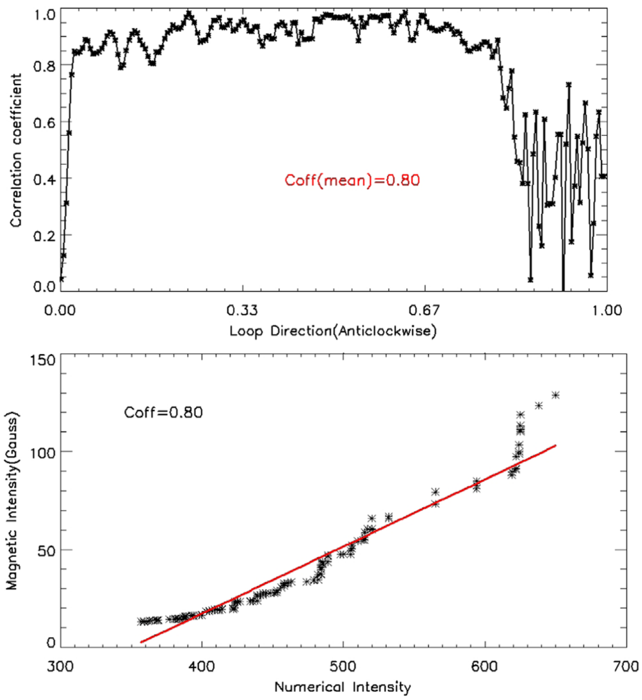

Figure 7. Upper: correlation distribution between the coronal brightness and magnetic field intensity along the direction of the loops in Figure 3. Each point represents the correlation coefficient between the two red dotted lines (X-axis direction), and there are 10 pixels used in the calculation for each point. Lower: the dependence of the coronal brightness on the magnetic field intensity between the two red dotted lines in the right panel of Figure 3, and the red line is a linear fitting to these scatter points.

From Figure 5, we can find that the profile of the correlation coefficients peaks at 1.103 $R_\odot$, where is the location with the most overlapped zones between the top of the loop and the 1.103 $R_\odot$ layer (see Figure 3). When lower than this layer of 1.1 $R_\odot$, the coefficient values increase monotonously, and when higher than 1.1 $R_\odot$ the coefficients decrease monotonously. In order to obtain more details about the value variations of "Coff" (i.e., the correlation coefficient between coronal brightness and magnetic field intensity) with height for each layer in yellow line in Figure 3, we show them in Figure 6. "h" represents the height, and the maximum coefficient is 0.82 found at 1.103 $R_\odot$. The red line is the fitted profile by a linear fit function.

Nonetheless, observations of the coronal loops could also provide information on the coronal magnetic field through magnetic field models (Lin & Forbes 2000; Lagg et al. 2007; Landi et al. 2020), and the study of magnetic field intensities associated with coronal loops has been significantly advanced. Numerous detailed investigations, such as the important information about the internal structuring of coronal loops comes from the joint analysis of the photospheric and coronal magnetic field (e.g., Yang et al. 2020a, 2020b); magnetic flux cancellation at the loop feet drives a significant heating mechanism for the hottest and brightest coronal loops (e.g., Reale 2014); directly compare the coronal loop topology with the magnetic field parameters (e.g., Schad et al. 2016); determine the magnetic field in coronal loops by using observations of coronal loop oscillations (e.g., Wang et al. 2007; Chen 2009; Li et al. 2021)). Significant advances in measurements of the magnetic field are expected to be made in the near future so that we could accurately extract the information between the actual topology of a coronal magnetic field and the intensity characteristic of a coronal loop.

We further investigate with the identified coronal loops in Figure 3. Let us start with the analysis of brightness and magnetic field intensity along the identified loops. At first, we take the median brightness, based on the 10 pixels evenly-distributed in each loop cross-section, as the tangential distribution along the loop. Then, the distribution of the coronal brightness is plotted from one set of footpoints to the other one (Y-axis direction) in Figure 7. "Coff(mean)" represents the average correlation coefficient calculated from the above distribution along the Y-axis direction is 0.80. The results clearly show that the correlation coefficients are positive and increasing quickly toward 1 and the maximum values occurs near the loop-top regions. The results imply that the high-temperature coronal emissions and the magnetic field intensity are closely correlated at their "middle" sections, i.e., about 70% full length centered the apex. On the other hand, the correlation coefficients are in some degree close to zero near the two root parts (i.e., $Y = 0.0$ and 1.0) of the coronal loops. It is well established that the structure of the solar atmosphere is full of complex plasma in which magnetic and plasma pressure play interchanging roles for dominance. The ratio of gas pressure to magnetic pressure is described by the plasma β (Gary 2001). In the PFSS extrapolation model, we suppose that the emission of plasma is in hydrostatic equilibrium along magnetic field loop and the magnetic pressure dominates over the plasma pressure. Nevertheless, the gas pressure actually dominates over the magnetic pressure in the photosphere at the base of the field loops (Gary & Alexander 1999). Gary (2001) showed that plasma β varies with height in the solar atmosphere complicatedly.

One statistical study indicates that the correlation coefficients can vary with latitude, and reach the greatest positive value within $\pm 40°$ (Badalyan 2013). In order to obtain a more detailed understanding of the "Coff" situation varies with latitude, we plan to analyze the distribution of the correlation with increasing radial height and the selected latitude zones are selected to a range of $\pm 40°$. In this work, the correlation was studied for a fixed heliocentric distance above the solar limb at low latitudes. Here, we show the dependence of the coronal brightness on magnetic field intensity within $\pm 40°$ latitudes at the solar equator on 2013 November 15 for 12 lower heights for pursuing higher confidence of data analysis (see Figure 8).

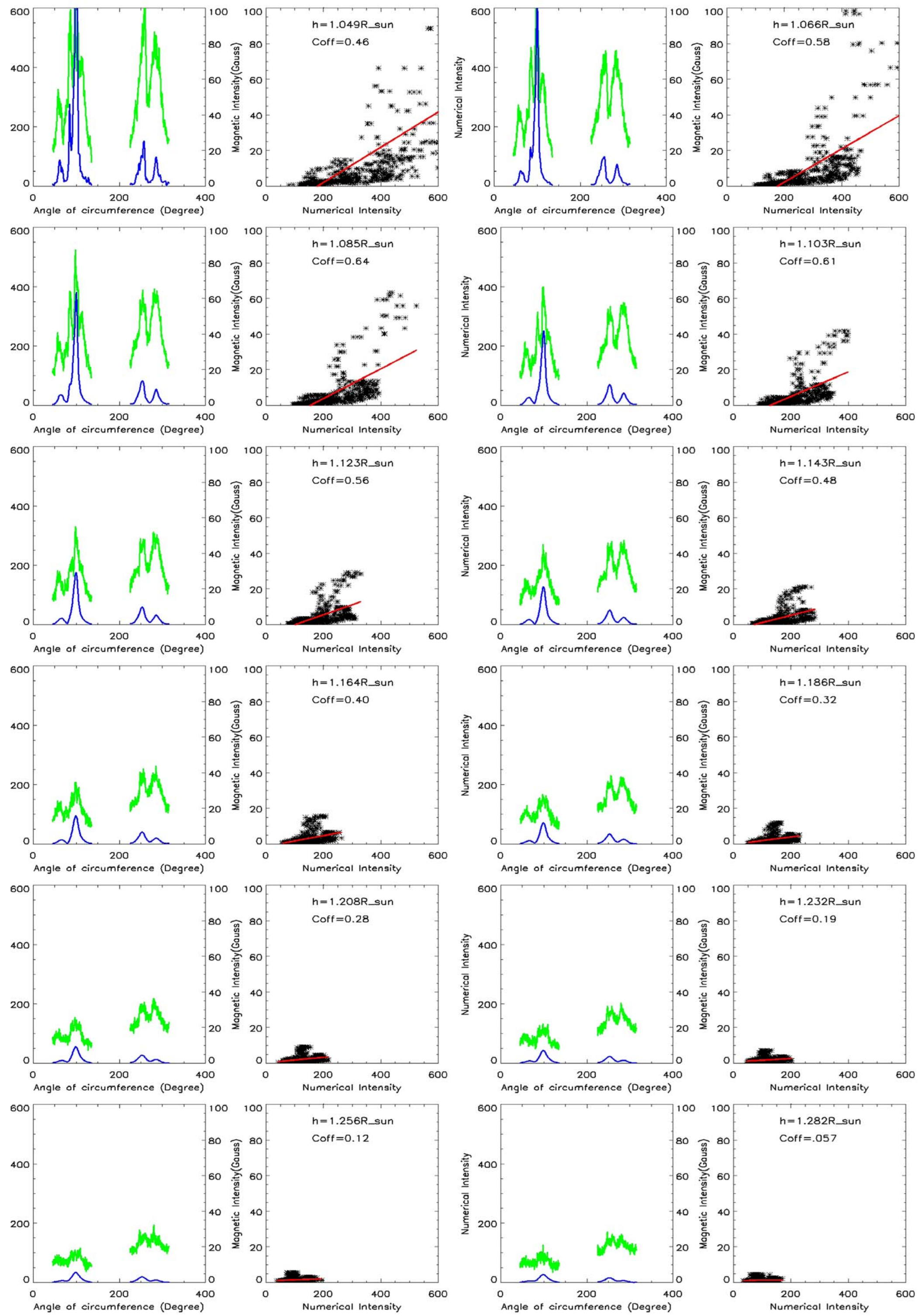

Figure 8. Plots comparing the observed brightness (green lines) with the extrapolated magnetic field intensity (blue lines) within $\pm 40^{\circ}$ latitudes at the solar equator with the heights of the heliocentric layers ("h" is the radial height). Measurements of the brightness plotted against the coronal magnetic field intensity are marked with black symbols, the red line indicates the fitted profile by a linear fit function, "Coff" represents the correlation coefficient between coronal brightness and magnetic field intensity.

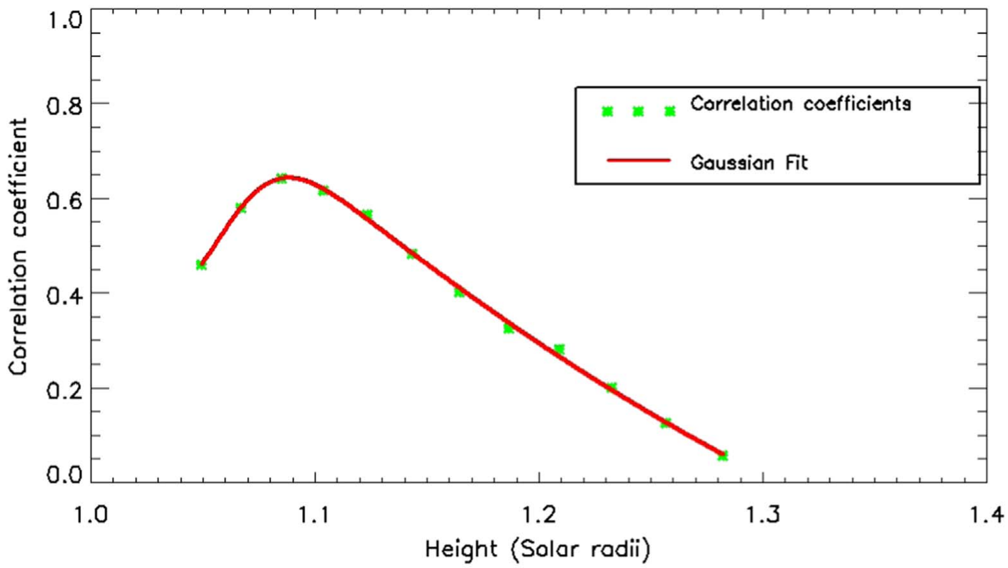

Figure 9. Correlation coefficients for between the coronal green line brightness and the magnetic field intensity within ±40° latitudes at the solar equator with the heights of the heliocentric layers in Figure 8. The red line indicates the fitted profile by a linear combination of a Gaussian and a quadratic function.

The observed brightness and the extrapolated magnetic intensity have been plotted as a function of the position angle from the Solar North along the arc in clockwise for each height. According to the results, although the observed brightness and the extrapolated intensity decrease significantly with the height which may cause large data error, the correlation coefficients larger than 0.6 still appear at around 1.1 $R_{\odot}$ (see Figure 9). The result strongly confirms that the large-scale brightness distribution of the coronal green line image matches well with the structure of the magnetic field including non-active regions.

It is worthy to study further the evolution of the correlation coefficient with radial height within different latitudes. In order to obtain a more detailed study, we use a sequence of the observations over an entire Carrington Rotation. Obridko & Shelting (1999) ever presented the correlation coefficients at near-polar latitudes and found them slightly negative, while we here use the data except for the polar zones. Figure 10 shows the distribution of the correlation between the observed brightness and the extrapolated magnetic field intensity for CR 2143 (2013 November 3–November 30). The coronal brightness and the extrapolated magnetic field are both selected within the same latitude zones from ±20° to ±70°. Again, all the distributions of the correlation coefficients for different latitude zones show agreements with the above results, with the maximum values appeared around 1.1 $R_{\odot}$.

4. Discussion and Conclusions

In this paper, we have shown the close relationship between the brightness in the coronal green line and the theoretical magnetic field intensity using data from the 10 cm coronagraph and the PFSS model. The coronal magnetic fields are calculated from the PFSS model based on the synoptic magnetograms, and we construct a two-dimensional image of the magnetic field intensity in the POS from 1.03 to 1.3 solar radii above the solar center. It is found that the correlation coefficients vary with height in different latitude zones represent the same tendency, and the height of 1.1 $R_{\odot}$ seems to be a particular layer in the corona. To investigate the magnetic field structure of the identified coronal loops, a coronal loop identification method based on the phase congruency theory (Li et al. 2017) is used to extract these loop systems. The results are summarized as follows:

1. For small-scale coronal bright feature, a maximum correlation coefficient 0.82 is found at height 1.1 $R_{\odot}$ at the top of a closed loop system, confirming the close relationship between the strong coronal green line brightness and magnetic field intensity (Figure 5).
2. For the extracted magnetic field intensity at the corresponding loop positions, we investigate the correlation between the coronal loop brightness and the magnetic field intensity and its distribution along the coronal loop. We find that the distribution of the correlation coefficient along the loop from one footpoint to the other one, finding the values are positive and increasing toward 1 quickly with the increase of the height.
3. For latitudes within ±40° we also find the maximum correlation coefficients larger than 0.6 to appear at the height 1.1 $R_{\odot}$ (Figure 8).
4. For more extended latitude zones covering from within ±20° to ±70° and for one longer period with a

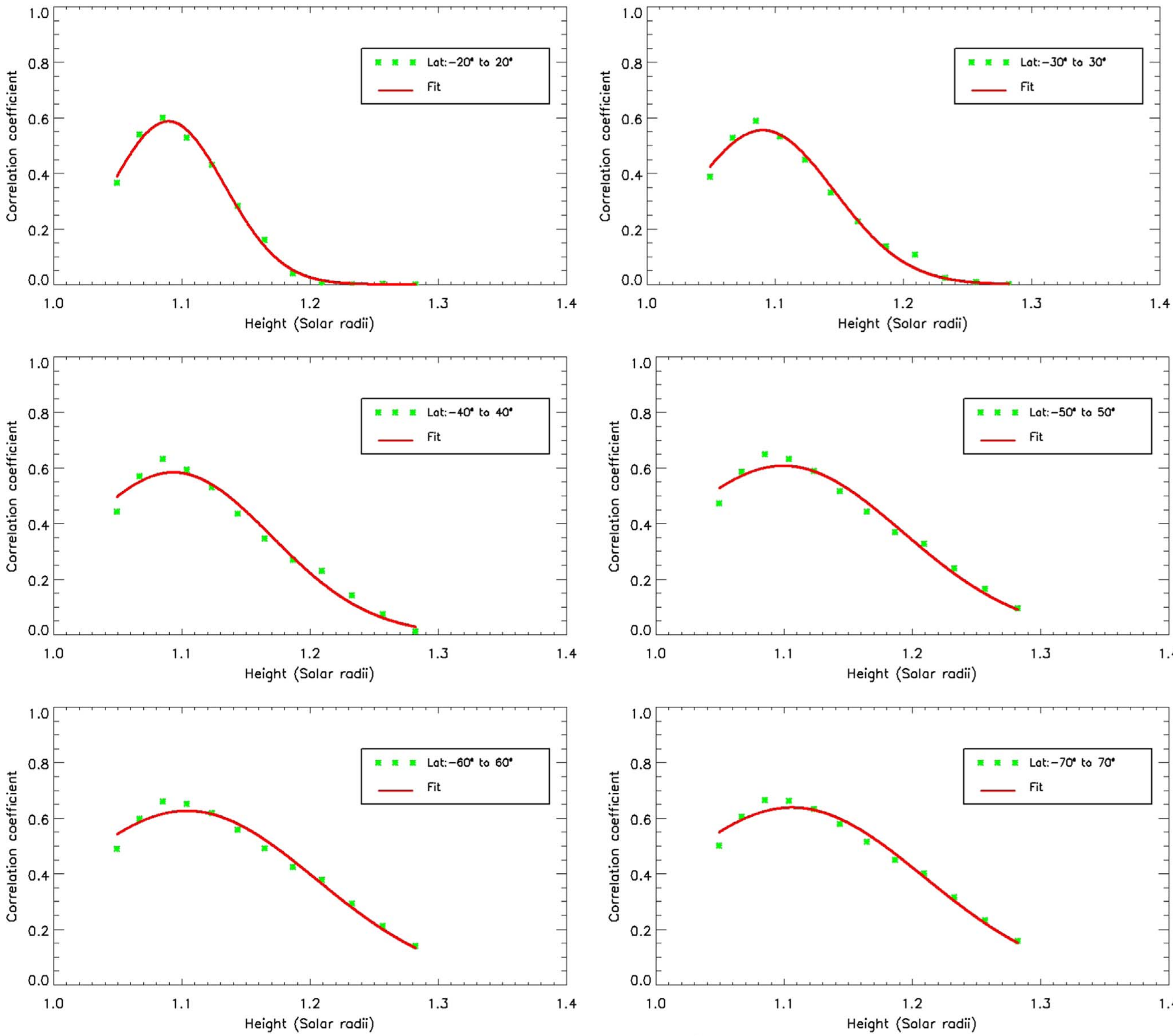

Figure 10. For six different latitude off-limb zones at different heights with one Solar Carrington Rotation period. The red solid lines are the fitted Gaussian function profiles.

whole CR spanning 27 days, the results still show the highest correlation at 1.1 $R_{\odot}$. Moreover, all the coefficient profiles show a Gaussian function profile (Figure 10).

Moreover, we find that average correlation coefficient as high as 0.80 along the coronal loops, the correlation coefficients are high (all are larger than 0.8) at the loop-tops. The tendency for a weaker correlation at the loop footpoints suggests that coronal heating mechanisms at loop's lower parts should be different from that of the loop upper parts. It is deduced that for the heating of the closed loops, both DC (dissipation of currents) and AC (dissipation of Alfvén and magnetosonic waves) mechanisms should act simultaneously on the whole closed loop system while the DC mechanisms dominate in the loop-top regions. We need to use more coronal green line data to derive reliable scaling laws relevant to coronal heating and to test various theoretical models for coronal fields for next studies. Interestingly, Squire et al. (2022) recently argued with their six-dimensional simulations that the proposed "helicity barrier" effect can be helpful to well unify these two ideas, and their results suggest that the helicity barrier could contribute to key observed differences between the fast and slow wind streams. However, it is unclear whether the height of 1.1 $R_{\odot}$ found in this paper is a key place for the helicity barrier to best function, which can be further studied for future simulations.

Since the maximum correlation coefficient appears around the top of the coronal arched structures, if the closed coronal arched structure is opened for some reason, then the hot plasma confined in the dense loop system (Vaiana et al. 1968) will be released and accelerated by the coronal magnetic field nearby. The height $1.1R_{\odot}$ should be important as the site of the source for the origin of the low-speed solar wind from the low solar corona (Neupert et al. 1992).

Acknowledgments

We sincerely thank the SDO team for the use of their observations; we also thank Prof. Sakurai,T and his NAOJ team for the 10 cm coronagraph instrument supplied to us. This work is supported by the National Natural Science Foundation of China under grants 11873090, 12173086, 11873092, U2031148 and the CAS "Light of West China" Program. We acknowledge for the data resources from the National Space Science Data Center, National Science & Technology Infrastructure of China (http://www.nssdc.ac.cn).

References

Badalyan, O. G. 2013, ARep, 57, 222
Badalyan, O. G., & Obridko, V. N. 2004, ARep, 48, 678
Badalyan, O. G., & Obridko, V. N. 2006, SoPh, 238, 271
Brooks, D. H., Warren, H. P., & Landi, E. 2021, ApJL, 915, L24
Chen, B., Shen, C., Gary, D. E., et al. 2020, NatAs, 4, 1140
Chen, P. 2009, ScChG, 52, 1785
Chen, Y., Tian, H., Su, Y., et al. 2018, ApJ, 856, 21
Chen, Y., Li, W., Tian, H., et al. 2021a, ApJ, 920, 116
Chen, Y., Liu, X., Tian, H., et al. 2021b, ApJL, 918, L13
Gary, G. A. 2001, SoPh, 203, 71
Gary, G. A., & Alexander, D. 1999, SoPh, 186, 123
Gregory, S. G., Donati, J. F., Morin, J., et al. 2012, ApJ, 755, 97
Gregory, S. G., Jardine, M., Gray, C. G., & Donati, J. F. 2010, RPPh, 73, 126901
Guhathakurta, M., Fisher, R. R., & Altrock, R. C. 1993, ApJL, 414, L145
Guhathakurta, M., Rottman, G. J., Fisher, R. R., Orrall, F. Q., & Altrock, R. C. 1992, ApJ, 388, 633
Habbal, S. R., Druckmüller, M., Morgan, H., et al. 2010, ApJ, 708, 1650
Ichimoto, K., Noguchi, M., Tanaka, N., et al. 1999, PASJ, 51, 383
Ji, H., Cao, W., & Goode, P. R. 2012, ApJL, 750, L25
Ji, H., Hashim, P., Hong, Z., et al. 2021, RAA, 21, 179
Jiang, C., Feng, X., Wu, S. T., & Hu, Q. 2013, ApJL, 771, L30
Klimchuk, J. A. 2002, in ASP Conf. Ser., 277, Stellar Coronae in the Chandra and XMM-NEWTON Era, ed. F. Favata & J. J. Drake (San Francisco, CA: ASP), 321
Lagg, A., Woch, J., Solanki, S. K., & Krupp, N. 2007, A&A, 462, 1147
Landi, E., Hutton, R., Brage, T., & Li, W. 2020, ApJ, 904, 87
Lemen, J. R., Title, A. M., Akin, D. J., et al. 2012, SoPh, 275, 17
Li, H.-b., Zhao, M.-y., & Liu, Y. 2017, ChA&A, 41, 357
Li, H., Feng, H., Shen, Y., et al. 2021, ApJ, 922, 224
Li, W., Grumer, J., Yang, Y., et al. 2015, ApJ, 807, 69
Li, W., Yang, Y., Tu, B., et al. 2016, ApJ, 826, 219
Liang, Y., Qu, Z. Q., Chen, Y. J., et al. 2021, MNRAS, 503, 5715
Lin, H. 2009, in ASP Conf. Ser., 405, Solar Polarization 5: In Honor of Jan Stenflo, ed. S. V. Berdyugina, K. N. Nagendra, & R. Ramelli (San Francisco, CA: ASP), 413
Lin, H., Penn, M. J., & Tomczyk, S. 2000, ApJL, 541, L83
Lin, J., & Forbes, T. G. 2000, JGR, 105, 2375
Liu, Y. 2009, Ann. Geophys., 27, 2771
Liu, Y., & Lin, H. 2008, ApJ, 680, 1496
Liu, Y., & Shen, Y. 2009, ScChG, 52, 1696
Liu, Y., Zhang, X., Song, T., et al. 2021, in 10th Int. Symp. on Advanced Optical Manufacturing and Testing Technologies: Large Mirror and Telescopes, 12070, ed. C.-H. Rao et al. (International Society for Optics and Photonics (SPIE)), 94
Nakariakov, V. M., & Kolotkov, D. Y. 2020, ARA&A, 58, 441
Neupert, W. M., Brosius, J. W., Thomas, R. J., & Thompson, W. T. 1992, ApJL, 392, L95
Nived, V. N., Scullion, E., Doyle, J. G., et al. 2022, MNRAS, 509, 5523
Obridko, V. N., & Shelting, B. D. 1999, SoPh, 187, 185
Pesnell, W. D., Thompson, B. J., & Chamberlin, P. C. 2012, SoPh, 275, 3
Qu, Z. Q., Dun, G. T., Chang, L., et al. 2017, SoPh, 292, 37
Reale, F. 2014, LRCA, 11, 4
Sakurai, T. 1981, SoPh, 69, 343
Sakurai, T. 2012, in ASP Conf. Ser., 454, Hinode-3: The 3rd Hinode Science Meeting, ed. T. Sekii, T. Watanabe, & T. Sakurai (San Francisco, CA: ASP), 439
Sakurai, T., Ichimoto, K., Raju, K. P., & Singh, J. 2002, SoPh, 209, 265
Schad, T. A., Penn, M. J., Lin, H., & Judge, P. G. 2016, ApJ, 833, 5
Schrijver, C. J., & De Rosa, M. L. 2003, SoPh, 212, 165
Shen, C., Chen, B., Reeves, K. K., et al. 2022, NatAstron, 6, 317
Shen, Y., Liu, Y. D., Chen, P. F., & Ichimoto, K. 2014, ApJ, 795, 130
Shen, Y., Tang, Z., Miao, Y., Su, J., & Liu, Y. 2018, ApJL, 860, L8
Squire, J., Meyrand, R., Kunz, M. W., et al. 2022, NatAstron, 69, 69
Stakhiv, M., Lepri, S., & Landi, E. 2015, in Solar Heliospheric and INterplanetary Environment (SHINE2015), 61
Stakhiv, M., Lepri, S. T., Landi, E., Tracy, P., & Zurbuchen, T. H. 2016, ApJ, 829, 117
Tan, B.-L., Karlický, M., Mészárosová, H., & Huang, G.-L. 2016, RAA, 16, 82
Tian, H., McIntosh, S. W., Wang, T., et al. 2012, ApJ, 759, 144
Vaiana, G. S., Reidy, W. P., Zehnpfennig, T., van Speybroeck, L., & Giacconi, R. 1968, Sci, 161, 564
Wang, T., Innes, D. E., & Qiu, J. 2007, ApJ, 656, 598
Wang, Y. M., Sheeley, N. R. J., Hawley, S. H., et al. 1997, ApJ, 485, 419
Wiegelmann, T., & Sakurai, T. 2021, LRCA, 18, 1
Wilson, J. M. 1869, Natur, 1, 139
Xin, Y.-X., Bai, J.-M., Lun, B.-L., et al. 2020, RAA, 20, 149
Xu, Z., Jiang, Y., Yang, J., Yang, B., & Bi, Y. 2016, ApJL, 820, L21
Yang, Z., Tian, H., Tomczyk, S., et al. 2020a, ScChE, 63, 2357
Yang, Z., Bethge, C., Tian, H., et al. 2020b, Sci, 369, 694
Yu, S., Chen, B., Reeves, K. K., et al. 2020, ApJ, 900, 17
Zhao, J., Gibson, S. E., Fineschi, S., et al. 2021, ApJ, 912, 141
Zhao, J., Gibson, S. E., Fineschi, S., et al. 2019, ApJ, 883, 55
Zhao, M. Y., Liu, Y., Elmhamdi, A., et al. 2018, SoPh, 293, 1
Zhao, M. Y., Liu, Y., Elmhamdi, A., et al. 2014, MNRAS, 443, 1955
Zhu, R., Tan, B., Su, Y., et al. 2021, ScChE, 64, 169
Zhu, X., & Wiegelmann, T. 2019, A&A, 631, A162